DIRECT SIMULATION OF TURBULENCE IN THE FLOW DRIVEN BY ROTATING AND TRAVELING MAGNETIC FIELDS

Jörg Stiller
Institut für Luft- und Raumfahrttechnik,
Technische Universität Dresden
D-01062 Dresden
joerg.stiller@tu-dresden.de

Kristina Koal
Institut für Luft- und Raumfahrttechnik,
Technische Universität Dresden
D-01062 Dresden
kristina.koal@tu-dresden.de

ABSTRACT

This paper presents results from a numerical study on electromagnetic stirring using rotating and traveling magnetic fields. Direct simulations of the flow in a cylindrical container were performed using a spectral-element/Fourier discretization of the magnetohydrodynamic equations in the low-frequency/low-induction limit.

In addition to the application of the single fields, the superposition with either well separated or equal frequencies was studied. Although a deeper investigation is still to be done, our results confirm that the latter case results in a strongly three-dimensional flow promising favorable mixing properties when compared with the other configurations.

INTRODUCTION

Electromagnetic flow control is important in crystal growth and metallurgic processes. We are interested in the latter, where various types of time-varying fields are applied to enhance the mixing of the melt. For an overview on this topic we refer to (Tsavaras and Brody, 1984), (Davidson, 1999) and (Stefanescu, 2002).

Typically, rotating or traveling magnetic fields (in short RMF and TMF) are used for stirring. In the first case, the configuration resembles an AC electric motor where the rotating field causes a torque acting on the rotor. In stirring the role of the rotor is adopted by the melt. Consequently, the RMF drives a swirling motion. In closed containers this primary flow is accompanied by a weak meridional circulation driven by the Bödewadt layers developing at the end walls (Davidson, 1992). During the solidification of alloys the RMF promotes the so-called columnar-to-equiaxed transition and thus leads to a finer, nearly isotropic material structure (Roplekar and Dantzing, 2001, Eckert et al. 2005). Unfortunately it turned out that the RMF-driven flow fails to homogenize the melt in the whole volume and may even cause adverse side effects such as increased macrosegregation (Nikrityuk et al. 2006a).

An alternative approach is to use traveling fields, which – like a linear motor or induction pump – cause a traction into a specified direction. In a cylindrical container the TMF generates a meridional circulation in the form of a toroidal vortex. Although flow control by traveling fields is widespread, scientific investigations are virtually limited to the laminar regime and its stability (Ramachandran et al. 2000, Grants and Gerbeth, 2004, Medina et al., 2004, Yesilyurt et al., 2004).

The circumstance that the bulk flow is azimuthal for the RMF and meridional for the TMF has inspired a number of attempts to enhance mixing by using a combination of these fields, e.g. (Denisov et al., 2003) and (Taniguchi et al., 2003). Except for preliminary results reported by Cramer et al. (2003) and Stiller et al. (2006), known scientific investigations are restricted to the axisymmetric laminar case (Gelfgat et al. 1999, Abricka et al. 2002).

In the present study we consider the turbulent flow driven by rotating and traveling fields as well as the superposition of these fields with either separate or equal frequencies. In the first case we assume that interference effects can be neglected, whereas they become even dominant in the second. Direct numerical simulations are employed to investigate the flow features. Within this paper the focus is set on the mean flow topology, the distribution of turbulent kinetic energy, the turbulent vortex structure and their consequences for the mixing efficiency.

MATHEMATICAL MODEL

Configuration

We consider the isothermal flow of an incompressible fluid with density ϱ, kinematic viscosity ν, and electric conductivity σ in an electrically non-conducting cylinder with radius R and height $H = 2R$. The configuration including the applied magnetic fields is sketched in Fig. 1. Since typical applications of electromagnetic stirring use low-frequency fields, shielding effects are neglected here. Furthermore, the magnitude of fluid velocity $\mathbf{u}$ is small compared to the phase velocity of the magnetic fields such that the induced fields can be ignored as well. These assumptions lead to the so-called low-frequency/low-induction approximation, which results in a decoupling and considerable simplification of the electrodynamic problem.

Rotating magnetic field

The RMF is given by

$$\mathbf{B}_\mathrm{R} = B_\mathrm{R}[\cos(\varphi - \omega_\mathrm{R} t)\mathbf{e}_r - \sin(\varphi - \omega_\mathrm{R} t)\mathbf{e}_\varphi] \qquad (1)$$

where B_R is the induction and ω_R the angular frequency.

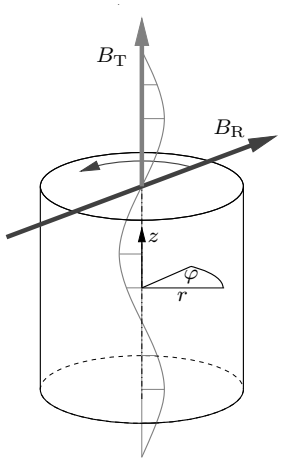

Figure 1: Configuration.

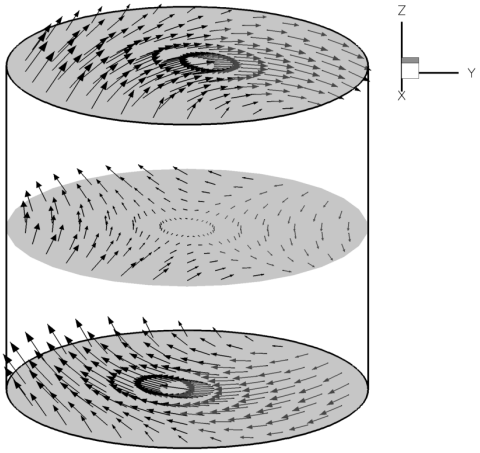

Figure 2: Electromagnetic body force for the case $\omega_\mathrm{R} = \omega_\mathrm{T}$, $Ta = F = 10^6$ and $I = 2.185 \times 10^6$.

The current density is

$$\mathbf{j}_\mathrm{R} = \sigma(\mathbf{E}_\mathrm{R} - \nabla\Phi_\mathrm{R}) = \sigma\omega_\mathrm{R} B_\mathrm{R} R \begin{pmatrix} \hat{j}_r \cos(\varphi - \omega_\mathrm{R} t) \\ \hat{j}_\varphi \sin(\varphi - \omega_\mathrm{R} t) \\ \hat{j}_z \cos(\varphi - \omega_\mathrm{R} t) \end{pmatrix} \quad (2)$$

where $\mathbf{E}_\mathrm{R}$ is the induced electric field and Φ_R the potential (Gorbachev et al. 1974),

$$\hat{j}_r = -\sum_{n=1}^{\infty} c_n \lambda_n \frac{J_0(\frac{\lambda_n r}{R}) - J_2(\frac{\lambda_n r}{R})}{2} \sinh(\tfrac{\lambda_n z}{R}), \quad (3)$$

$$\hat{j}_\varphi = \sum_{n=1}^{\infty} c_n \lambda_n \frac{J_0(\frac{\lambda_n r}{R}) + J_2(\frac{\lambda_n r}{R})}{2} \sinh(\tfrac{\lambda_n z}{R}), \quad (4)$$

$$\hat{j}_z = \frac{r}{R} - \sum_{n=1}^{\infty} c_n \lambda_n J_1(\tfrac{\lambda_n r}{R}) \cosh(\tfrac{\lambda_n z}{R}), \quad (5)$$

J_k the Bessel functions, λ_n the zeros of J_1', and

$$c_n = 2/[\lambda_n(\lambda_n^2 - 1) J_1(\lambda_n) \cosh(\lambda_n)]. \quad (6)$$

Traveling magnetic field

We constrain ourselves to long-wave fields, for which the wave number satisfies the relation $k_\mathrm{T} H \ll 1$. In this case the TMF induction and the induced current are given by

$$\mathbf{B}_\mathrm{T} = B_\mathrm{T} \left[\frac{k_\mathrm{T} r}{2} \sin(k_\mathrm{T} z - \omega_\mathrm{T} t) \mathbf{e}_r + \cos(k_\mathrm{T} z - \omega_\mathrm{T} t) \mathbf{e}_z \right] \quad (7)$$

and

$$\mathbf{j}_\mathrm{T} = \sigma\omega_\mathrm{T} B_\mathrm{T} \frac{r}{2} \sin(k_\mathrm{T} z - \omega_\mathrm{T} t) \mathbf{e}_\varphi \quad (8)$$

respectively.

ELECTROMAGNETIC BODY FORCE

The simultaneous application of an RMF and a TMF yields the body force

$$\begin{aligned} \mathbf{f} &= \mathbf{j}_\mathrm{R} \times \mathbf{B}_\mathrm{R} + \mathbf{j}_\mathrm{T} \times \mathbf{B}_\mathrm{T} + (\mathbf{j}_\mathrm{R} \times \mathbf{B}_\mathrm{T} + \mathbf{j}_\mathrm{T} \times \mathbf{B}_\mathrm{R}) \\ &= \mathbf{f}_\mathrm{R} + \mathbf{f}_\mathrm{T} + \mathbf{f}_\mathrm{I}. \end{aligned} \quad (9)$$

The individual contributions of the rotating and traveling field oscillate with the double frequencies, $2\omega_\mathrm{R}$ and $2\omega_\mathrm{T}$, respectively. Because these are much higher than the characteristic flow frequency, $\omega_\mathrm{F} = u_\mathrm{max}/R$, the forces can be approximated by their mean values. The corresponding expressions can be arranged in the form

$$\mathbf{f}_\mathrm{R} = \frac{\rho\nu^2}{R^3}\ Ta\, \hat{j}_z\, \mathbf{e}_\varphi, \quad \mathbf{f}_\mathrm{T} = \frac{\rho\nu^2}{R^3}\ \frac{F}{2} \frac{r^2}{R^2}\, \mathbf{e}_z \quad (10)$$

where

$$Ta = \frac{\sigma\omega_\mathrm{R} B_\mathrm{R}^2 R^4}{2\varrho\nu^2}, \quad F = \frac{\sigma\omega_\mathrm{T} B_\mathrm{T}^2 k_\mathrm{T} R^5}{4\varrho\nu^2} \quad (11)$$

is the Taylor number of the RMF and the forcing parameter of the TMF, respectively.

The interaction force $\mathbf{f}_\mathrm{I}$ consists of two parts that oscillate with the combination frequencies $\omega_\mathrm{R} + \omega_\mathrm{T}$ and $\omega_\mathrm{R} - \omega_\mathrm{T}$, respectively. We are interested in two special cases: In the first case $\Delta\omega = |\omega_\mathrm{R} - \omega_\mathrm{T}|$ is assumed to be large in comparison with ω_F and, hence, $\mathbf{f}_\mathrm{I}$ can be neglected. As the second case we consider $\omega_\mathrm{R} = \omega_\mathrm{T} = \omega$. While the part of $\mathbf{f}_\mathrm{I}$ oscillating with $\omega_\mathrm{R} + \omega_\mathrm{T}$ is still negligible, the other gives rise to the steady, three-dimensional forcing

$$\mathbf{f}_\mathrm{I} = \frac{\rho\nu^2}{R^3}\ I \begin{pmatrix} \hat{j}_\varphi \sin(\psi) \\ -\hat{j}_z \frac{k_\mathrm{T} r}{2} \sin(\psi) - \hat{j}_r \cos(\psi) \\ -\frac{1}{2}\frac{r}{R} \sin(\psi) - \hat{j}_\varphi \frac{k_\mathrm{T} r}{2} \cos(\psi) \end{pmatrix} \quad (12)$$

where $\psi = \varphi - k_\mathrm{T} z$ and

$$I = \sqrt{\frac{2\,Ta\,F}{k_\mathrm{T} R}} = \frac{\sigma\omega B_\mathrm{R} B_\mathrm{T} R^4}{2\varrho\nu^2}. \quad (13)$$

A vector plot of the total body force in the second case ($\Delta\omega = 0$) is shown in Fig. 2.

Flow equations

Using the scales R, R^2/ν, ν/R, and $\varrho\nu^2/R^3$ for length, time, velocity, and body force, the nondimensional flow equations write

$$\nabla \cdot \mathbf{u} = 0, \quad (14)$$

$$\partial_t \mathbf{u} + \nabla \cdot \mathbf{u}\mathbf{u} = -\nabla p + \nabla^2 \mathbf{u} + \mathbf{f}. \quad (15)$$

NUMERICAL METHOD

All simulations were performed using the spectral element / Fourier code *semtex*, which employs quadrilateral nodal elements in the meridional semi-plane coupled with

Table 1: Cases and parameters.

Case	Ta	F	I	N_φ
RMF	10^6	0	–	256
TMF	0	4×10^6	–	320
S-1	10^6	4×10^6	–	256
S-2	10^6	10^6	2.185×10^6	512

trigonometric expansions in the azimuth. For details of the method we refer to (Blackburn and Sherwin 2004).

The implementation of the body force was verified by comparison to an implementation in *Mathematica* and various test cases, including the analytic solution for the RMF-driven flow in an infinite cylinder and the linear instability of TMF-driven flow (Grants and Gerbeth 2004).

RESULTS

Direct numerical simulations were carried out for RMF and TMF with different forcing parameters (cf. Table 1). The computational domain was discretized using 25×50 spectral elements of order 11 and $N_\varphi = 256$ to 512 meridional planes, corresponding to 128 to 256 Fourier modes, respectively. The grid spacing in the radial and axial directions varied from $\Delta^+ \leq 0.2$ near the walls to $\Delta^+ \approx 3.5$ in the core region.

Case RMF: Rotating Magnetic Field

The flow features obtained in this case (see Fig. 3) agree well with earlier results for $H/2R = 1.5$ (Stiller et al., 2006). The mean flow is governed by the swirling motion induced by the RMF body force. The meridional circulation driven by the top and bottom Bödewadt layers leads to a homogenization of the flow, but is too weak to provide for an efficient mixing (Nikrityuk et al. 2006b). One may anticipate that this function is adopted by the Taylor-Görtler vortices, which are visualized in Fig. 3(c) using the λ_2 criterion. These vortices represent the main turbulence mechanism and lead to an intensive mass and momentum transfer in the radial and axial directions. However, as the azimuthal fluctuations contain contain only about one fifth of the turbulence energy, the exchange is less effective in the φ direction. Another drawback from the perspective of stirring is that the vortices are largely confined to the near wall region $r > 0.8$.

Case TMF: Traveling Magnetic Field

Figure 4 depicts the average velocity, turbulent kinetic energy and vortices for $F = 4 \times 10^6$. The mean flow resembles a smooth, toroidal vortex, whereas the instantaneous flow is fully turbulent and regularly changes its topology. The turbulent fluctuations share about one half of the total kinetic energy, which is an exceptional high degree in shear flows. Apart from a certain preference of the axial direction, the vortices are randomly oriented and cover the whole domain, thus rendering the TMF a promising choice for mixing applications.

Case S-1: Linear Superposition

In this case the rotating and traveling fields considered before were superimposed such that interference effects are negligible. In practice this can be achieved, e.g., by choosing $\omega_\mathrm{T} = 2\omega_\mathrm{R}$. The naive idea behind this approach is that the superposition would result in a favorable combination of the different mixing mechanisms that are present in the flow driven either by the RMF or TMF alone. Because the maximum velocity in the RMF case is almost two times higher than in the TMF case, it is not surprising that the azimuthal swirling motion prevails. Figure 5 reveals that the topology of the meridional flow is almost equivalent to the RMF case. The only qualitative change due to the traveling field is the break of vertical symmetry, which is caused by the redistribution of angular momentum towards the upper lid. As a result, the maximum of azimuthal velocity is shifted from the neutral plane to the top of the cylinder and increased to 3410 from 3070 in the RMF case. The magnitude of vertical velocity increased as well, but remains about two thirds below the value obtained in the TMF case.

Figures 5(b,c) show that the turbulence properties are also very similar to the RMF case, such that the "linear" superposition of the fields considered here does not promise any significant advantage. It remains an open question, however, in which way the flow pattern changes when the TMF forcing is intensified.

Case S-2: Superposition with Equal Frequencies

In contrast to the previous case, both fields oscillate with the same frequency here. Furthermore, the TMF forcing was reduced by a factor of four. These changes result in a completely different flow topology: Figure 6 reveals that the main flow is composed of a swirling motion driven by the RMF and a circulation that appears as a single vortex in the plane $x = 0$. One side effect of this circulation is the redistribution of angular momentum and a deformation of the azimuthal flow. Although the thorough assessment of statistical properties is still progress, we conclude that flow is strongly three-dimensional also in the mean. Moreover, all velocity components are approximately of the same order. These features promise favorable mixing properties in comparison with the purely RMF- and TMF-driven flows, which are inherently two-dimensional. On the other hand, the static asymmetry of the flow may cause adverse effects in some applications. In casting, for example, the inhomogeneous melt flow may lead to a significant distortion of the solidification front with unpredictable consequences for the structure of the ingot.

Finally, Fig. 7 shows the instantaneous vortex structure for the same snapshot. Most vortices are located at the top left and the bottom right, which are the locations where the circulation driven by the interaction force encounters the lids. In contrast to the previous cases no preferred orientation can be identified.

CONCLUSIONS

The flow driven by rotating and traveling magnetic fields and two qualitatively different combinations of these fields was studied by means of direct numerical simulation.

The imposition of a RMF yields a homogeneously rotating flow with Taylor-Görtler vortices as the main turbulence mechanism. As a consequence, the RMF provides for efficient stirring, but limited mixing. The meridional circulation driven by the TMF is less stable, which results in a lower mean velocity and a remarkably high contribution of turbulence to the total kinetic energy. Therefore, the TMF is clearly better suited for mixing than the RMF.

The linear (interference-free) superposition of both fields

leads to a dominance of the RMF, if the individual forcing parameters are comparable. From the perspective of mixing, the resulting flow offers no significant advantage. A completely different flow pattern arises, when both fields oscillate with the same frequency. The resulting flow is genuinely three-dimensional in its mean as well as in the turbulent part. Unfortunately, the presumably high mixing efficiency is counterbalanced by the inhomogeneous transport properties due to the static asymmetry of the flow. It may be conjectured that a better compromise is achieved, if the frequencies of the applied fields are slightly different, i.e., $0 < \Delta\omega \ll \omega_F$.

ACKNOWLEDGMENTS

We thank Prof. H. M. Blackburn for providing the flow solver *semtex*. Financial support from Deutsche Forschungsgemeinschaft in frame of the Collaborative Research Center SFB 609 is gratefully acknowledged. The computations were performed on an SGI Altix system based on a grant from ZIH at TU Dresden.

REFERENCES

Abricka, M., Gelfgat, Yu., and Krūmiņš, J., 2002, "Influence of combined electromagnetic fields on the heat/mass transfer in the Bridgman process," *Energy Conversion and Management*, Vol. 43, pp. 327-333.

Blackburn H. M., and Sherwin, S. J., 2004, "Formulation of a Galerkin spectral element Fourier method for three-dimensional incompressible flows in cylindrical geometries," *J. Comp. Phys.*, Vol. 197, pp. 759-778.

Cramer, A., Eckert, S., Heinzelmann, C., Zhang, C., and Gerbeth, G., 2003, "Efficient melt mixing due to the combined action of a rotating and a travelling magnetic field," *Proc. 4th Int. Conf. on Electromagnetic Processing of Materials*, Lyon, France, pp. 359-365.

Davidson, P. A., 1992, "Swirling flow in an axisymmetric cavity of arbitrary profile driven by a rotating magnetic field," *J. Fluid Mech.*, Vol. 245, pp. 669-699.

Davidson, P. A., 1999, "Magnetohydrodynamics in materials processing," *Ann. Rev. Fluid Mech.*, Vol. 31, pp. 273-300.

Denisov, S., Kripchenko, S., Kolesnichenko, I., and Yudakov, A., 2003, "MHD-stirrer for cylindrical moulds of continuous casting machines fabricated aluminium alloy ingots," *Proc. 4th Int. Conf. on Electromagnetic Processing of Materials*, Lyon, France, pp. 178-184.

Eckert, S., Willers, B., Nikrityuk, P. A., Eckert, K., Michel, U., and Zouhar, G., 2005, "Application of a rotating magnetic field during solidification of Pb-Sn alloys during directional solidification: consequences on the CET," *Mater. Sci. Eng. A*, Vol. 413-414, 211-216.

Gelfgat, Yu., Krūmiņš, J., and Abricka, M., 1999, "Motion of an electrically conducting fluid in a cylindrical volume acted on by superimposed rotating and travelling magnetic fields," *Magnetohydrodynamics*, Vol. 36, pp. 3-16.

Gorbachev, L. P., Nikitin, N. V., and Ustinov, A.L., 1974, "Magnetohydrodynamic rotation of an electrically conducting liquid in a cylindrical vessel of finite dimensions," *Magnetohydrodynamics*, Vol. 10, pp. 406-414.

Grants, I. and Gerbeth, G., 2001, "Stability of axially symmetric flow driven by a rotating magnetic field in a cylindrical cavity," *J. Fluid Mech.*, Vol. 431, pp. 407-426.

Grants, I. and Gerbeth, G., 2004, "Stability of melt flow due to a travelling magnetic field in a closed ampoule," *J. Cryst. Growth*, Vol. 269, pp. 630-638.

Medina, M., Du Terrail, Y., Durand, G., and Fautrelle, Y., 2004, "Channel segregation during solidification and the effects of an alternating traveling magnetic field," *Metallurgical and Materials Transactions B*, Vol. 35, pp. 743-754.

Nikrityuk, P.A., Eckert, K., and Grundmann, R., 2006a, "A numerical study of unidirectional solidification of a binary metal alloy under influence of a rotating magnetic field," *Int. J. Heat Mass Transfer*, Vol. 49, pp. 1501-1515.

Nikrityuk, P.A., Eckert, K., and Grundmann, R., 2006b, "Axisymmetric modelling of the mixing of two miscible liquid metals driven by a rotating magnetic field," *Proc. Conference on Turbulence and Interactions TI2006*, Porquerolles, France, May 28 June 2, 2006.

Ramachandran, N., Mazuruk, K,. and Volz, M. P., 2000, "Use of traveling magnetic fields to control melt flow convection," *J. Jpn. Soc. Microgravity Appl.*, Vol. 17(2), pp. 98-103.

Stefanescu, D. M., 2002, "Science and Engineering of Casting Solidification," Kluwer Academic/Plenum Publishers New York.

Stiller, J., Fraňa, K., and Cramer, A., 2006, "Transitional and weakly turbulent flow in a rotating magnetic field," *Phys. Fluids*, Vol. 18, 074105.

Stiller. J., Koal, K., Fraňa, K., and Grundmann, R., 2006, "Stirring of Melts using Rotating and Traveling Magnetic Fields," *Proc.* 5^{th} *Int. Conf. on CFD in the Process Industries*, CSIRO Australia, Dec. 13-15.

Taniguchi, S., Maitake, K., Okubo, M., Ando, T., and Ueno, K., 2003, "Rotary stirring of liquid metal without free surface deformation by combination of rotational and vertical travelling magnetic fields - development of hybrid stirrer," *Proc. 4th Int. Conf. on Electromagnetic Processing of Materials*, Lyon, 14-17 Oct., pp. 339-343.

Tsavaras, A .A., and Brody, H. D., 1984, "Electromagnetic stirring and continuous casting achievements, problems and goals," *J. Metals*, Vol. 167, pp. 31-37.

Yesilyurt, S., Motakel, S., Grugel, R., and Mazuruk, K., 2004, "The effect of the traveling magnetic field (TMF) on the buoyancy-induced convection in the vertical Bridgman growth of semiconductors," *J. Cryst. Growth*, Vol. 263, pp. 80-89.

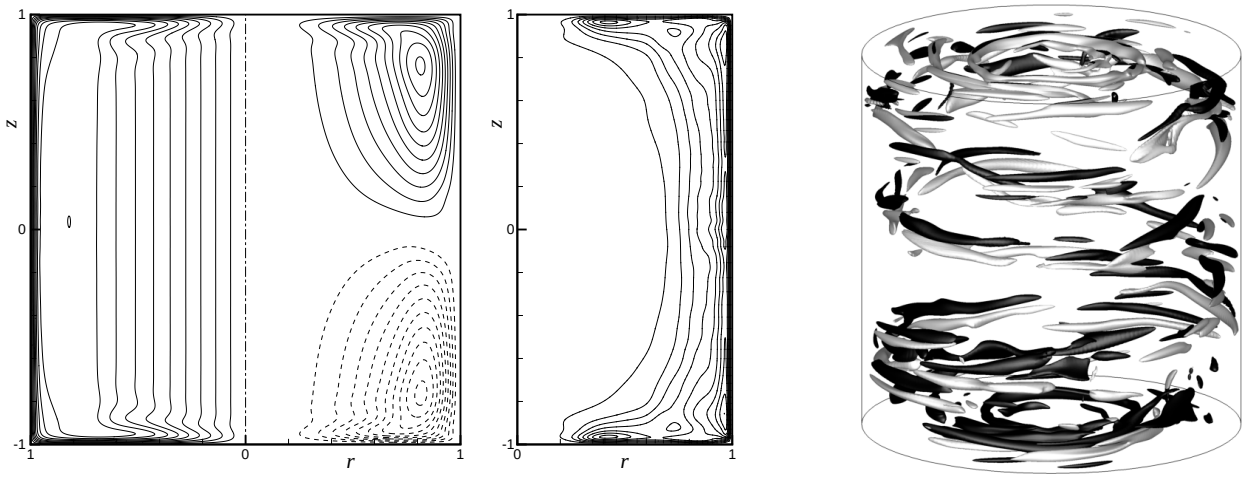

(a) $\bar{u}_\varphi$ contours (l), meridional streamlines (r). (b) k contours. (c) Instantaneous vortex structure.

Figure 3: RMF-driven flow at $Ta = 10^6$. Contour levels differ by 10% of the absolute extremum. Dashed lines correspond to negative values. Vortices are shaded according to the sign of azimuthal vorticity to indicate their sense of rotation.

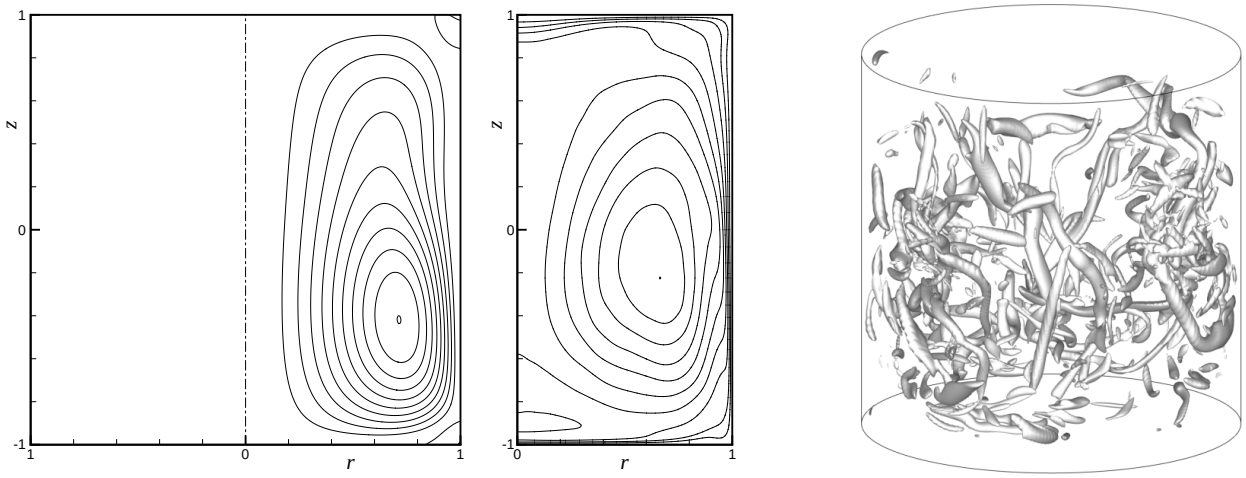

(a) Meridional streamlines (r), $\bar{u}_\varphi$ tends to zero. (b) k contours. (c) Instantaneous vortex structure.

Figure 4: TMF-driven flow at $F = 4 \times 10^6$.

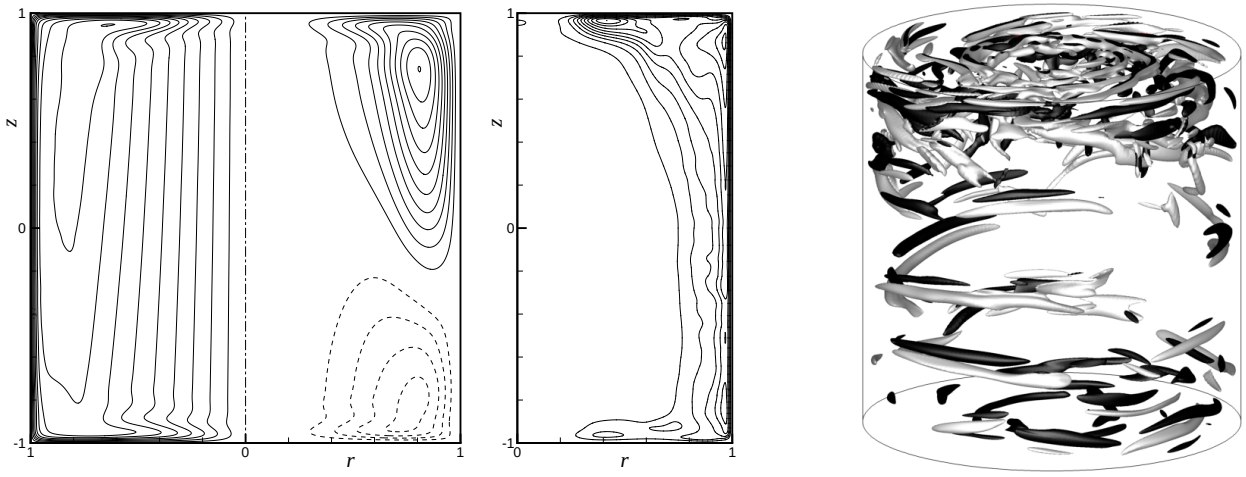

(a) $\bar{u}_\varphi$ contours (l), meridional streamlines (r). (b) k contours. (c) Instantaneous vortex structure.

Figure 5: Superposition of RMF and TMF with $Ta = 10^6$, $F = 4 \times 10^6$ and $\omega_\mathrm{R} \neq \omega_\mathrm{T}$.

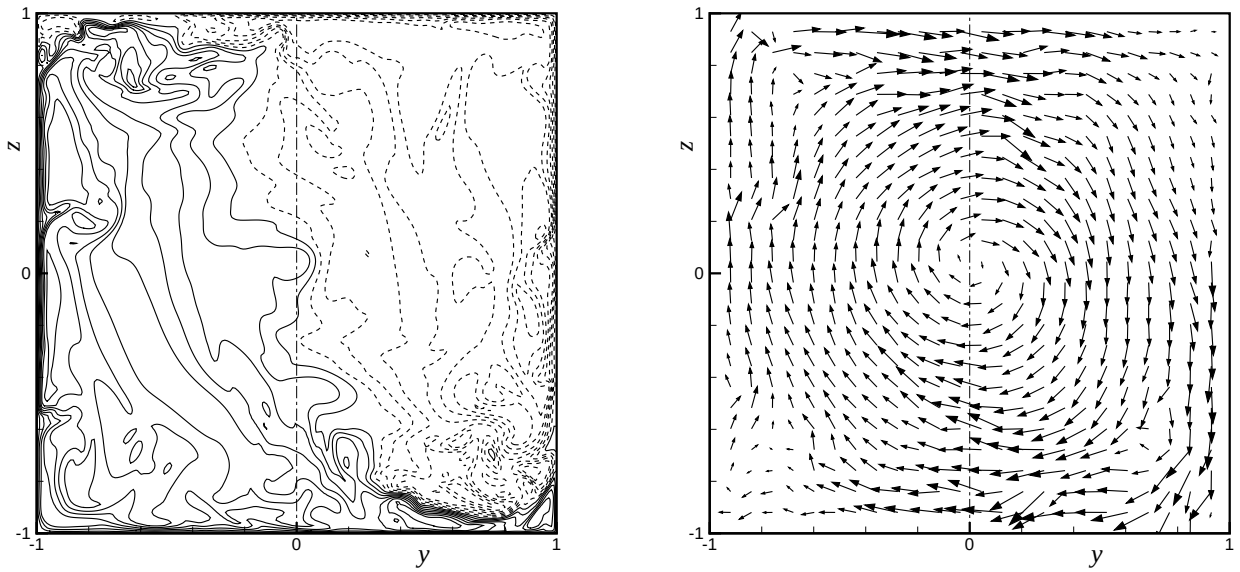

(a) Contours of u_x in the plane $x = 0$.

(b) Velocity vectors projected to the plane $x = 0$.

Figure 6: Snapshot of the flow for the case $Ta = 10^6$, $F = 10^6$ and $\omega_{\mathrm{R}} = \omega_{\mathrm{T}}$.

Figure 7: Vortex structure for the case $\omega_{\mathrm{R}} = \omega_{\mathrm{T}}$.